



Phenomenology of two-dimensional stably stratified turbulence under large-scale forcing

Abhishek Kumar, Mahendra K. Verma & Jai Sukhatme

To cite this article: Abhishek Kumar, Mahendra K. Verma & Jai Sukhatme (2017) Phenomenology of two-dimensional stably stratified turbulence under large-scale forcing, Journal of Turbulence, 18:3, 219-239, DOI: [10.1080/14685248.2016.1271123](https://doi.org/10.1080/14685248.2016.1271123)

To link to this article: <http://dx.doi.org/10.1080/14685248.2016.1271123>



Published online: 10 Jan 2017.



Submit your article to this journal [↗](#)



Article views: 83



View related articles [↗](#)



View Crossmark data [↗](#)

Phenomenology of two-dimensional stably stratified turbulence under large-scale forcing

Abhishek Kumar ^a, Mahendra K. Verma^a and Jai Sukhatme^b

^aDepartment of Physics, Indian Institute of Technology, Kanpur, India; ^bCentre for Atmospheric and Oceanic Sciences, Indian Institute of Science, Bangalore, India

ABSTRACT

In this paper, we characterise the scaling of energy spectra, and the interscale transfer of energy and enstrophy, for strongly, moderately and weakly stably stratified two-dimensional (2D) turbulence, restricted in a vertical plane, under large-scale random forcing. In the strongly stratified case, a large-scale vertically sheared horizontal flow (VSHF) coexists with small scale turbulence. The VSHF consists of internal gravity waves and the turbulent flow has a kinetic energy (KE) spectrum that follows an approximate k^{-3} scaling with zero KE flux and a robust positive enstrophy flux. The spectrum of the turbulent potential energy (PE) also approximately follows a k^{-3} power-law and its flux is directed to small scales. For moderate stratification, there is no VSHF and the KE of the turbulent flow exhibits Bolgiano–Obukhov scaling that transitions from a shallow $k^{-11/5}$ form at large scales, to a steeper approximate k^{-3} scaling at small scales. The entire range of scales shows a strong forward enstrophy flux, and interestingly, large (small) scales show an inverse (forward) KE flux. The PE flux in this regime is directed to small scales, and the PE spectrum is characterised by an approximate $k^{-1.64}$ scaling. Finally, for weak stratification, KE is transferred upscale and its spectrum closely follows a $k^{-2.5}$ scaling, while PE exhibits a forward transfer and its spectrum shows an approximate $k^{-1.6}$ power-law. For all stratification strengths, the total energy always flows from large to small scales and almost all the spectral indices are well explained by accounting for the scale-dependent nature of the corresponding flux.

ARTICLE HISTORY

Received 18 July 2016
Accepted 5 December 2016

KEYWORDS

Direct numerical simulation;
stratified turbulence

1. Introduction

Stable stratification with rotation is an important feature of geophysical flows [1]. The strength of stratification is usually measured by the non-dimensional parameter called Froude number (Fr), which is defined as the ratio of the time scale of gravity waves and the nonlinear time scale. Strong stratification has $Fr \ll 1$, while weak stratification has $Fr \geq 1$ [2]. In this paper, we restrict ourselves to two-dimensional (2D) stable stratification in a vertical plane [3,4], this allows us to explore a wide range of Fr and characterise the interscale transfer of energy and enstrophy, and the energy spectra in strongly, moderately, and weakly stratified scenarios.

Apart from a reduction in dimensionality, the 2D stratified system differs from the more traditional three-dimensional (3D) equations in that it lacks a vortical mode. Indeed, the decomposition of the 3D system into vortical and wave modes [2,5,6] has proved useful in studying stratified [7–11] and rotating-stratified [12–17] turbulence. The absence of a vortical mode implies that the 2D stratified system only supports nonlinear wave–wave mode interactions [18,19] (interestingly, 3D analogs that only support wave interactions have also been considered previously [20,21]). In a decaying setting, the initial value problem concerning the fate of a standing wave in 2D has been studied experimentally [22] and numerically [23,24]. The regime was that of strong stratification, and not only where the waves observed to break, this process was accompanied by a forward energy transfer due to nonlocal parametric subharmonic instability [23]. Further, at long times after breaking, the turbulence generated was characterised by a k_{\parallel}^{-3} scaling [24] (i.e. parallel to the direction of ambient stratification). Other decaying simulations, that focussed on the formation and distortion of fronts from an initially smooth profile, noted a self-similarity in the probability density function of the vorticity field as well as more of an isotropic $k^{-5/3}$ kinetic energy (KE) spectrum, though at early stages in the evolution of the system [25].

With respect to the forced problem, the case of random small-scale forcing has been well studied. Specifically, at moderate stratification, the 2D system developed a robust vertically sheared horizontal flow (VSHF; [13]) accompanied by an inverse transfer of KE and a $k^{-5/3}$ scaling [26]. For weak stratification, a novel flux loop mechanism involving the upscale transfer of KE (with $k^{-5/3}$ scaling) and the downscale transfer of potential energy (PE), also with $k^{-5/3}$ scaling, was seen to result in a stationary state [27]. In fact, moisture-driven strongly-stratified flows in 2D have also been seen to exhibit an upscale KE transfer with a $k^{-5/3}$ scaling [28]. Interestingly, large-scale forcing in the form of a temperature gradient has been examined experimentally. Specifically, using a soap film, Zhang *et al.* [29] reported scaling of density fluctuations at low frequencies with exponents $-7/5$ (Bolgiano scaling [30,31]) and -1 (Batchelor scaling [32]) for moderate and strong temperature gradients, respectively. Seychelles *et al.* [33] noted a similar scaling and the development of isolated coherent vortices on a curved 2D soap bubble.

For quasi-two-dimensional (quasi-2D) stably stratified turbulence (i.e. flows contained in a skewed aspect ratio box), Lindborg [34] performed simulations at the horizontal Froude numbers ranging approximately from 10^{-2} to 10^{-3} , i.e. in a very strongly stratified regime. It was observed that the horizontal kinetic and PE spectra followed $k_{\perp}^{-5/3}$ scaling (i.e. perpendicular to the ambient stratification), while the vertical kinetic and PE spectra followed k_{\parallel}^{-3} scaling [see also, 35,36]. Further, in this quasi-2D setting, Vallgren *et al.* [16] added rotation to strong stratification in an attempt to explain the observed atmospheric kinetic and PE spectra.

In the present work, we look at the relatively unexamined case of random forcing at large scales for 2D stably stratified turbulence. The flows are simulated using a pseudo-spectral code Tarang [37] for strongly, moderately and weakly stratified scenarios. For strong stratification, a VSHF (identified as internal gravity waves) emerges at large scales and coexists with small scale turbulence. The turbulent flow is characterised by a forward enstrophy cascade, zero KE flux, and a KE spectrum that scales approximately as k^{-3} . The PE spectrum also follows an approximate k^{-3} power-law with a scale-dependent flux of the form k^{-2} . At moderate stratification, there is no VSHF, and the KE spectrum shows a modified form of Bolgiano–Obukhov [30,31] scaling for 2D flows – approximately $k^{-11/5}$ at

large scales and k^{-3} at small scales in a similar manner as in 3D [38]. The KE flux also changes character with scale, and exhibits an inverse (forward) transfer at large (small) scales. The PE spectrum follows an approximate $k^{-1.64}$ scaling and its flux is weakly scale-dependent. Finally, for weak stratification, the KE flux is upscale for most scales and its spectrum is characterised by a -2.5 exponent. The PE flux continues to be downscale and its spectrum obeys an approximate $k^{-1.6}$ scaling. All exponents observed are well explained by taking into account the variable nature of the corresponding flux. Exceptions are the PE spectra for moderate and weak stratification whose scaling is little steeper than expected.

The outline of the paper is as follows. In Section 2, we describe the equations governing stably stratified flows and the associated parameters. In Section 3, we discuss the numerical details of our simulations. In the subsequent three subsections, we detail various kinds of flows observed for strongly stably stratified flows in Section 4.1, moderately stably stratified flows in Section 4.2, and weakly stably stratified flows in Section 4.3. Finally, we conclude in Section 5 with a summary and discussion of our results.

2. Governing equations

We employ the following set of equations to describe 2D stably stratified flows [39]:

$$\frac{\partial \mathbf{u}}{\partial t} + (\mathbf{u} \cdot \nabla) \mathbf{u} = -\frac{1}{\rho_0} \nabla p - \frac{\rho}{\rho_0} g \hat{z} + \nu \nabla^2 \mathbf{u} + \mathbf{f}_u, \quad (1)$$

$$\frac{\partial \rho}{\partial t} + (\mathbf{u} \cdot \nabla) \rho = -\frac{d\bar{\rho}}{dz} u_z + \kappa \nabla^2 \rho, \quad (2)$$

$$\nabla \cdot \mathbf{u} = 0, \quad (3)$$

where \mathbf{u} is the 2D velocity field, p is the pressure, ρ and ρ_0 are the the fluctuating and background densities, respectively, \hat{z} is the buoyancy direction while \hat{x} is the horizontal direction, \mathbf{f}_u is the external force field, g is the acceleration due to gravity, and ν and κ are the kinematic viscosity and thermal diffusivity, respectively. In the above description, we make the Boussinesq approximation under which the density variation of the fluid is neglected except for the buoyancy term. Also, $d\bar{\rho}/dz < 0$ due to stable stratification.

The linearised version of Equations (1)–(3) yields internal gravity waves for which the velocity and density fluctuate with the Brunt Väisälä frequency N defined using,

$$N^2 = -\frac{g}{\rho_0} \frac{d\bar{\rho}}{dz}. \quad (4)$$

The linearised equations also yield a dispersion relation for the internal gravity waves as

$$\Omega = N \frac{k_x}{k}, \quad (5)$$

where $k = \sqrt{k_x^2 + k_z^2}$.

For simplification, we convert density to units of velocity by a transformation [40]:

$$b = \frac{g}{N} \frac{\rho}{\rho_0}. \quad (6)$$

Thus, in terms of b , Equations (1) and (2) become

$$\frac{\partial \mathbf{u}}{\partial t} + (\mathbf{u} \cdot \nabla) \mathbf{u} = -\frac{1}{\rho_0} \nabla p - bN\hat{z} + \nu \nabla^2 \mathbf{u} + \mathbf{f}_u, \quad (7)$$

$$\frac{\partial b}{\partial t} + (\mathbf{u} \cdot \nabla) b = Nu_z + \kappa \nabla^2 b. \quad (8)$$

In the limiting case of $\nu = \kappa = 0$ and $\mathbf{f}_u = 0$, only the total energy

$$E = \frac{1}{2} \int (u^2 + b^2) d\mathbf{r} \quad (9)$$

is conserved. This is in contrast to the 2D inviscid Navier–Stokes equation that has two conserved quantities – the KE $\int d\mathbf{r}(u^2/2)$ and the enstrophy $\int d\mathbf{r}(\nabla \times \mathbf{u})^2/2$ [41]. Based on these two conservation laws, Kraichnan [41] deduced a dual energy spectrum for 2D hydrodynamic turbulence – $C_1 \Pi_u^{2/3} k^{-5/3}$ for $k < k_f$, and $C_2 \Pi_\omega^{2/3} k^{-3}$ for $k > k_f$. Here Π_u and Π_ω are the energy flux and enstrophy flux, respectively, k_f is the forcing wavenumber, and C_1 and C_2 are constants that have been estimated as 5.5–7.0 [42,43] and 1.3–1.7 [44,45], respectively.

The important nondimensional variables used for describing stably stratified flows are

$$\text{Prandtl number } \text{Pr} = \frac{\nu}{\kappa}, \quad (10)$$

$$\text{Rayleigh number } \text{Ra} = \frac{N^2 d^4}{\nu \kappa}, \quad (11)$$

$$\text{Reynolds number } \text{Re} = \frac{u_{\text{rms}} d}{\nu}, \quad (12)$$

$$\text{Froude number } \text{Fr} = \frac{u_{\text{rms}}}{Nd}, \quad (13)$$

$$\text{Richardson number } \text{Ri} = \frac{1}{\text{Fr}^2}, \quad (14)$$

$$\text{Buoyancy Reynolds number } \text{Re}_b = \text{ReFr}^2, \quad (15)$$

where u_{rms} is the rms velocity of flow, which is computed as a volume average. Note that the Rayleigh number is the ratio of the buoyancy and the viscous force, while the Richardson number is the ratio of the buoyancy and the nonlinearity $(\mathbf{u} \cdot \nabla) \mathbf{u}$.

It is convenient to work with nondimensional equations using box height d as a length scale, Nd as a velocity scale, and $-(d\bar{\rho}/dz)d$ as the density scale, which leads to $\mathbf{u} = \mathbf{u}'Nd$, $\rho = -\rho'(d\bar{\rho}/dz)d$, $\mathbf{x} = \mathbf{x}'d$, and $t = t'/N$. Hence the nondimensionalised version of Equations (1)–(3) is

$$\frac{\partial \mathbf{u}'}{\partial t'} + (\mathbf{u}' \cdot \nabla') \mathbf{u}' = -\nabla' p' - \rho' \hat{z} + \sqrt{\frac{\text{Pr}}{\text{Ra}}} \nabla'^2 \mathbf{u}' + \mathbf{f}'_u, \quad (16)$$

$$\frac{\partial \rho'}{\partial t'} + (\mathbf{u}' \cdot \nabla') \rho' = u'_z + \frac{1}{\sqrt{\text{RaPr}}} \nabla'^2 \rho', \quad (17)$$

$$\nabla' \cdot \mathbf{u}' = 0. \quad (18)$$

In the above set of equations, the control parameters of the system are Ra, Pr, and ε , the energy supply rate by the external forcing \mathbf{f}'_u (see Equation (37) for details of forcing scheme). The Reynolds number Re and the Froude number Fr are the response parameters. We compute Re and Fr using following formula:

$$\text{Re} = \frac{u'_{\text{rms}} d}{\nu} = u'_{\text{rms}} \frac{Nd^2}{\nu} = u'_{\text{rms}} \sqrt{\frac{\text{Ra}}{\text{Pr}}}, \quad (19)$$

$$\text{Fr} = \frac{u'_{\text{rms}}}{Nd} = u'_{\text{rms}}. \quad (20)$$

Note that, in the dimensionless form the Froude number is the rms velocity of the fluid. From this point onward we drop the primes on the variables for convenience.

In this paper we solve the above equations numerically, and study the energy spectra and fluxes in the regimes of strong stratification, moderate stratification, and weak stratification. Note that the KE spectrum $E_K(k)$, the horizontal KE spectrum $E_{K_h}(k)$, the vertical KE spectrum $E_{K_v}(k)$, and the PE spectrum $E_p(k)$ are defined as

$$E_K(k) = \sum_{k-1 < k' \leq k} \frac{1}{2} |u(\mathbf{k}')|^2, \quad (21)$$

$$E_{K_h}(k) = \sum_{k-1 < k' \leq k} \frac{1}{2} |u_x(\mathbf{k}')|^2, \quad (22)$$

$$E_{K_v}(k) = \sum_{k-1 < k' \leq k} \frac{1}{2} |u_z(\mathbf{k}')|^2, \quad (23)$$

$$E_p(k) = \sum_{k-1 < k' \leq k} \frac{1}{2} |\rho(\mathbf{k}')|^2. \quad (24)$$

In Fourier space, the equation for the KE $E_K(k)$ of the wavenumber shell of radius k is derived from Equation (16) as [46,47]

$$\frac{\partial E_K(k)}{\partial t} = T_K(k) + F_B(k) + F_{\text{ext}}(k) - D(k), \quad (25)$$

where $T_K(k)$ is the energy transfer rate to the shell k due to nonlinear interaction, and $F_B(k)$ and $F_{\text{ext}}(k)$ are the energy supply rates to the shell from the buoyancy and external forcing \mathbf{f}_u , respectively, i.e.

$$F_B(k) = \sum_{|\mathbf{k}|=k} \Re(\langle u_z(\mathbf{k}) \rho^*(\mathbf{k}) \rangle), \quad (26)$$

$$F_{\text{ext}}(k) = \sum_{|\mathbf{k}|=k} \Re(\langle \mathbf{u}(\mathbf{k}) \cdot \mathbf{f}_u^*(\mathbf{k}) \rangle). \quad (27)$$

In Equation (25), $D(k)$ is the viscous dissipation rate defined by

$$D(k) = \sum_{|\mathbf{k}|=k} 2\nu k^2 E_K(k). \quad (28)$$

The KE flux $\Pi_K(k_0)$, which is defined as the KE leaving a wavenumber sphere of radius k_0 due to nonlinear interaction, is related to the nonlinear interaction term $T_K(k)$ as

$$\Pi_K(k) = - \int_0^k T_K(k) dk. \quad (29)$$

Under a steady state [$\partial E_K(k)/\partial t = 0$], using Equations (25) and (29), we deduce that

$$\frac{d}{dk} \Pi_K(k) = F_B(k) + F_{\text{ext}}(k) - D(k) \quad (30)$$

or

$$\Pi_K(k + \Delta k) = \Pi_K(k) + (F_B(k) + F_{\text{ext}}(k) - D(k)) \Delta k. \quad (31)$$

In computer simulations, the KE flux, $\Pi_K(k_0)$, is computed by the following formula, using *mode-to-mode* energy transfer procedure [48,49],

$$\Pi_K(k_0) = \sum_{k>k_0} \sum_{p \leq k_0} \delta_{\mathbf{k}, \mathbf{p}+\mathbf{q}} \Im([\mathbf{k} \cdot \mathbf{u}(\mathbf{q})][\mathbf{u}^*(\mathbf{k}) \cdot \mathbf{u}(\mathbf{p})]). \quad (32)$$

Dar *et al.* [48] presented a very efficient technique to compute the above flux using a pseudo-spectral method. Specifically, Equation (32) is written in terms of *truncated* variables $\mathbf{u}^>$ and $\mathbf{u}^<$, and reads

$$\Pi_K(k_0) = \Im \left[\sum_{k>k_0} k_j \{u_i^>(\mathbf{k})\}^* \sum_{p \leq k_0} u_j(\mathbf{k} - \mathbf{p}) u_i^<(\mathbf{p}) \right]. \quad (33)$$

Here,

$$\mathbf{u}^>(\mathbf{k}) = \begin{cases} 0 & \text{if } k \leq k_0, \\ \mathbf{u}(\mathbf{k}) & \text{if } k > k_0, \end{cases}$$

and

$$\mathbf{u}^<(\mathbf{p}) = \begin{cases} \mathbf{u}(\mathbf{p}) & \text{if } p \leq k_0, \\ 0 & \text{if } p > k_0. \end{cases}$$

The second summation of Equation (33) (over p) is the convolution sum, which is computed using the fast Fourier transform [48,49]. For clarity, Figure 1 illustrates the triad interaction involved in an energy flux computations.

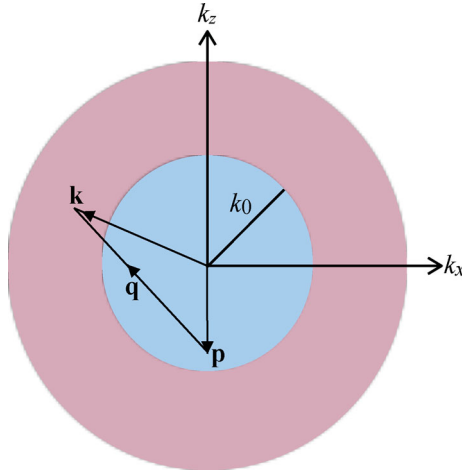


Figure 1. Schematic diagram of the energy flux from a wavenumber sphere of radius k_0 . The blue (light) region denotes the modes inside the sphere, and the red (dark) region the modes outside the sphere.

Similarly, the enstrophy flux $\Pi_\omega(k_0)$ and PE flux $\Pi_P(k_0)$ are the enstrophy and the PE leaving a wavenumber sphere of radius k_0 , respectively. The formulae to compute these quantities are

$$\Pi_\omega(k_0) = \sum_{k > k_0} \sum_{p \leq k_0} \delta_{\mathbf{k}, \mathbf{p} + \mathbf{q}} \Im([\mathbf{k} \cdot \mathbf{u}(\mathbf{q})][\omega^*(\mathbf{k})\omega(\mathbf{p})]), \quad (34)$$

$$\Pi_P(k_0) = \sum_{k > k_0} \sum_{p \leq k_0} \delta_{\mathbf{k}, \mathbf{p} + \mathbf{q}} \Im([\mathbf{k} \cdot \mathbf{u}(\mathbf{q})][\rho^*(\mathbf{k})\rho(\mathbf{p})]). \quad (35)$$

Note that the total energy flux $\Pi_{\text{Total}}(k)$ is defined as

$$\Pi_{\text{Total}}(k) = \Pi_K(k) + \Pi_P(k). \quad (36)$$

In the above expression, the prefactors are unity due to nondimensionalisation. In the following sections, we compute the aforementioned spectra and fluxes using the steady-state numerical data.

3. Simulation method

We solve Equations (16)–(18) numerically using a pseudo-spectral code Tarang [37]. In brief, the code employs a fourth-order Runge–Kutta method for time stepping, the Courant–Friedrichs–Lewy condition to determine the time step Δt , and 2/3 rule for dealiasing. Finally, we use periodic boundary conditions on both sides of a square box of dimension $2\pi \times 2\pi$.

Table 1. Parameters of our direct numerical simulations (DNS): Froude number Fr ; grid resolution; Rayleigh number Ra ; energy supply rate ε ; Richardson number Ri ; Reynolds number Re ; buoyancy Reynolds number Re_b ; anisotropy ratio $A = \langle u_{\perp}^2 \rangle / \langle u_{\parallel}^2 \rangle$; and $k_{\max}\eta$, where k_{\max} is the maximum wavenumber and η is the Kolmogorov length. We kept the Prandtl number $Pr = 1$ for all our runs.

Fr	Grid	Ra	ε	Ri	Re	Re_b	A	$k_{\max}\eta$
0.16	512^2	10^9	10^{-6}	40	5.0×10^3	1.3×10^2	38	2.8
0.31	512^2	10^8	10^{-4}	11	3.1×10^3	3.0×10^2	38	3.7
0.37	8192^2	10^{10}	0.01	7.3	3.7×10^4	5.1×10^3	3.4	4.9
0.45	512^2	10^8	0.01	4.9	4.5×10^3	9.1×10^2	4.2	1.4
0.73	2048^2	10^8	0.1	1.9	7.3×10^3	4.0×10^3	1.6	3.8
1.1	2048^2	10^8	0.3	0.8	1.1×10^4	1.3×10^4	1.4	3.3

Table 2. Values of the kinetic energy E_K , the potential energy E_p , E_p/E_K , the kinetic energy dissipation rate ϵ_K , the potential energy dissipation rate ϵ_p , and ϵ_p/ϵ_K at different Froude number for all runs.

Fr	E_K	E_p	E_p/E_K	ϵ_K	ϵ_p	ϵ_p/ϵ_K
0.16	1.3×10^{-2}	8.8×10^{-4}	0.1	2.2×10^{-6}	1.7×10^{-7}	0.1
0.31	4.7×10^{-2}	4.5×10^{-3}	1.0	2.2×10^{-5}	6.2×10^{-6}	0.3
0.37	6.8×10^{-2}	3.8×10^{-2}	0.6	4.9×10^{-4}	2.8×10^{-3}	5.7
0.45	1.0×10^{-1}	3.8×10^{-2}	0.4	1.2×10^{-3}	2.9×10^{-3}	2.4
0.73	3.0×10^{-1}	2.0×10^{-1}	0.7	5.3×10^{-3}	2.7×10^{-2}	5.1
1.1	6.0×10^{-1}	4.0×10^{-1}	0.6	9.2×10^{-3}	7.7×10^{-2}	8.4

Since the system is stable, we apply random large-scale forcing in the band $2 \leq k \leq 4$ to obtain a statistically steady turbulent flow using the following scheme:

$$\mathbf{f}_u(\mathbf{k}) = Ae^{i\Phi} \begin{pmatrix} \cos \vartheta \\ -\sin \vartheta \end{pmatrix}, \quad (37)$$

where ϑ is the angle between $\hat{\mathbf{z}}$ and \mathbf{k} , Φ is the random phase in $[0, 2\pi]$ with zero mean, and

$$A = \sqrt{\frac{2\varepsilon}{n_f \Delta t}}. \quad (38)$$

Here, ε is the total energy supply rate and n_f is the total number of modes inside the forcing wavenumber band.

In Tables 1 and 2 we list the set of parameters for which we performed our simulations. We employ grid resolutions of 512^2 to 8192^2 , the higher ones for higher Reynolds number. The Rayleigh number of our simulations ranges from 10^8 to 10^{10} , while the Reynolds number ranges from 5000 to 3.7×10^4 . All our simulations are fully resolved since $k_{\max}\eta > 1$, where η is the Kolmogorov length scale, and k_{\max} is the maximum wavenumber attained in direct numerical simulation (DNS) for a particular grid resolution. Note that the energy supply rate, ε , is greater than the viscous dissipation rate, ϵ_u , with the balance getting transferred to the PE via buoyancy ($\rho g u_z / \rho_0$).

The Froude numbers of our simulations are $Fr = 0.16, 0.31, 0.37, 0.45, 0.73$, and 1.1 ; the lowest Fr corresponds to the strongest stratification, while the largest Fr to the weakest

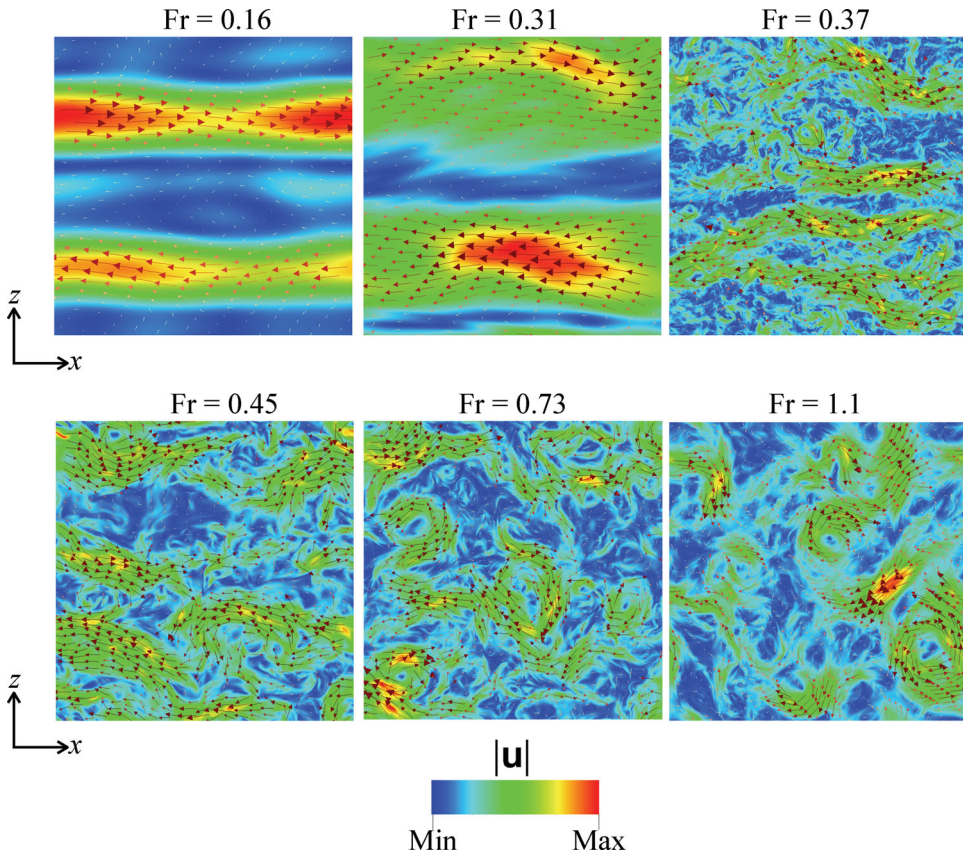


Figure 2. For $Fr = 0.16, 0.31, 0.37, 0.45, 0.73,$ and 1.1 , the density plots of the magnitude of velocity field with the velocity vector \mathbf{u} superposed on it in the x - z plane. For low Fr , fluctuations are suppressed along buoyancy direction. However, they grow gradually on the increase of Fr . We classify $Fr = 0.16, 0.31$ as strong stratification, 0.37 and 0.45 as moderate stratification, 1.1 as weak stratification, and 0.73 as transition between moderate and weak stratification.

stratification. We show in subsequent discussion that the flow behaviours in these regimes are very different. One of the major differences is the anisotropy that is quantified using an anisotropy parameter $A = \langle u_{\perp}^2 \rangle / \langle u_{\parallel}^2 \rangle$. For the strongest stratification with $Fr = 0.16$, $A \approx 38$ indicating a strong anisotropy. However, for the weakest stratification with $Fr = 1.1$, $A \approx 1.4$ indicating a near isotropy.

4. Results

We begin with a qualitative description of the flow profiles for the strongly, moderately, and weakly stratified regimes. In [Figure 2](#), we show the velocity vectors superposed on the magnitude of the velocity field. For strong stratification ($Fr = 0.16$), we observe two robust flow structures moving in the opposite directions, i.e. a VSHF [13]. On further increasing Fr to 0.31 , the streams widen and start to diffuse. In the moderately stratified regime ($Fr = 0.37, 0.45$), the streams break into filaments, and the flow becomes progressively disordered. Finally, for weak stratification ($Fr = 1.1$), the flow appears turbulent during which

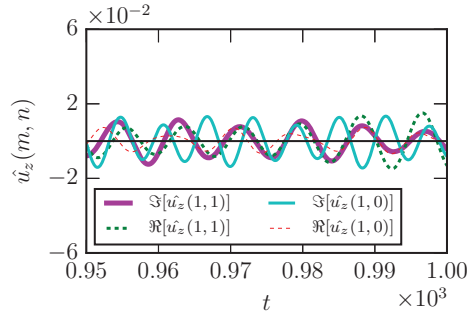


Figure 3. Time series of the real and imaginary parts of Fourier modes $\hat{u}_z(1, 1)$ and $\hat{u}_z(1, 0)$ for strong stratification ($Fr = 0.16$).

the aforementioned filaments tend to be wrapped into compact isolated vortices [50]. The transition from moderate to weak stratification occurs near $Fr = 0.73$.

4.1. Strong stratification

Here, we focus on the simulation with $Fr = 0.16$, $Re = 5000$, $Pr = 1$, $Ra = 10^9$, and forcing amplitude $\varepsilon = 10^{-6}$. The flow exhibits strong anisotropy as is evident from the ratio $A = \langle u_{\perp}^2 \rangle / \langle u_{\parallel}^2 \rangle = 38$. In fact, the flow exhibits wave-like behaviour that can be confirmed by studying the dominant Fourier modes.

We compute the most energetic Fourier modes in the flow and find the modes $(1, 0)$ and $(1, 1)$ to be the most dominant. Figure 3 shows the time series of the real and imaginary parts of $\hat{u}_z(1, 1)$ and $\hat{u}_z(1, 0)$ from which we extract the oscillation time period of these modes as approximately 8.4 and 6.5, and their frequencies as 0.75 and 0.97. These numbers match very well with the dispersion relation (Equation (5)), thus we interpret these structures to be internal gravity waves. Note that these robust flow structures moving in horizontal directions constitute the VSHF. We also observe that $\hat{\mathbf{u}}(0, n) \approx 0$ where n is an integer, so almost no energy is transferred to purely zonal flows. A natural vertical length scale that emerges in strongly stratified flows is U/f , where U is the magnitude of the horizontal flow and $f = N/2\pi$ [51]. With the present parameters, we see that this leads to VSHFs of size ~ 1 , which is in reasonable agreement with the bands seen in the first panel of Figure 2.

To explore the flow properties further, we compute the KE spectrum $E_K(k)$, and the KE and enstrophy fluxes. As shown in Figure 4(a), the KE at small scales (large k) is several orders of magnitude lower than that for low- k modes. Thus, even though small-scale turbulence is present in the system, the energy content of the large scale internal gravity waves is much larger than the sea of small-scale turbulence. The flux computations show that the KE flux $\Pi_K(k) \approx 0$ for $k > k_f$, but the enstrophy flux $\Pi_{\omega}(k)$ is positive and fairly constant (see Figure 4(b)). For these band of wavenumbers we observe that

$$E_K(k) \approx 1.0 \Pi_{\omega}^{2/3} k^{-3}, \quad (39)$$

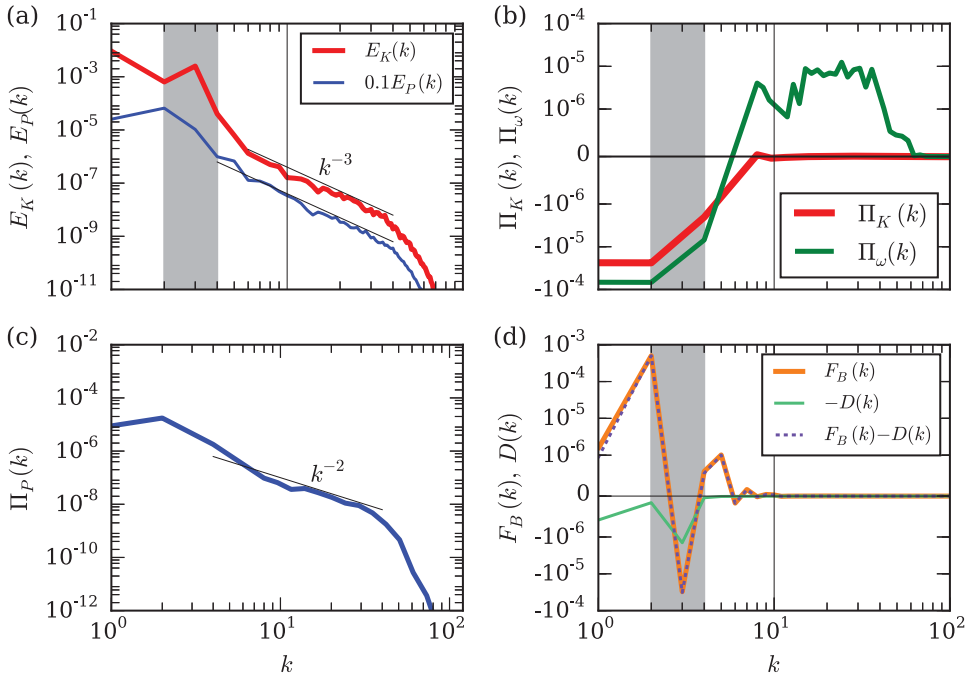


Figure 4. Strong stratification ($Fr = 0.16$): (a) KE and PE spectra; (b) KE flux $\Pi_K(k)$ and enstrophy flux $\Pi_\omega(k)$. The grey-shaded region shows the forcing band. The KE flux is zero for wavenumber $k \geq 10$; (c) PE flux $\Pi_P(k)$; (d) $F_B(k)$, $D(k)$, and $F_B(k) - D(k)$.

which is similar to the forward enstrophy cascade regime of 2D turbulence (including the prefactor) [44,45]. The aforementioned flux computations are also consistent with the fluxes reported for 2D turbulence [52–54].

In addition, we observe that the PE spectrum, $E_P(k)$, scales approximately as k^{-3} and the PE flux follows $\Pi_P(k) \sim k^{-2}$ (see Figure 4(a,c)). The k^{-3} scaling of the PE is in sharp contrast to the k^{-1} Batchelor spectrum for a passive scalar in 2D hydrodynamic turbulence in the wavenumber regimes with a forward enstrophy cascade [32,55]. Further, $\Pi_P(k)$ decreases rapidly with wavenumber, rather than being a constant as for a passive scalar. We demonstrate the consistency among these scalings of KE and PE as follows: the KE spectrum $E_K(k) \sim k^{-3}$ implies $u_k \sim k^{-1}$, substitution of which in the PE flux equation yields

$$\Pi_P \approx ku_k \rho_k^2 \sim k^{-2}. \quad (40)$$

Consequently, $\rho_k \sim k^{-1}$, and hence

$$E_P(k) \approx \frac{\rho_k^2}{k} \sim k^{-3}. \quad (41)$$

Also, Figure 4(d) shows the energy supply rate due to buoyancy $F_B(k)$ and the dissipation rate $D(k)$. The buoyancy is active at large scales only, and it is quite small for $k \geq 10$.

Given the anisotropic nature of the flow, we also compute the KE spectrum of the horizontal flow $E_{K_h}(k)$ and of the vertical flow $E_{K_v}(k)$, which are shown in Figure 5. As expected,

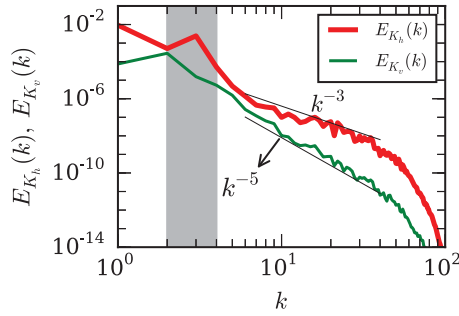


Figure 5. Plots for horizontal and vertical kinetic energy spectra for strong stratification ($Fr = 0.16$).

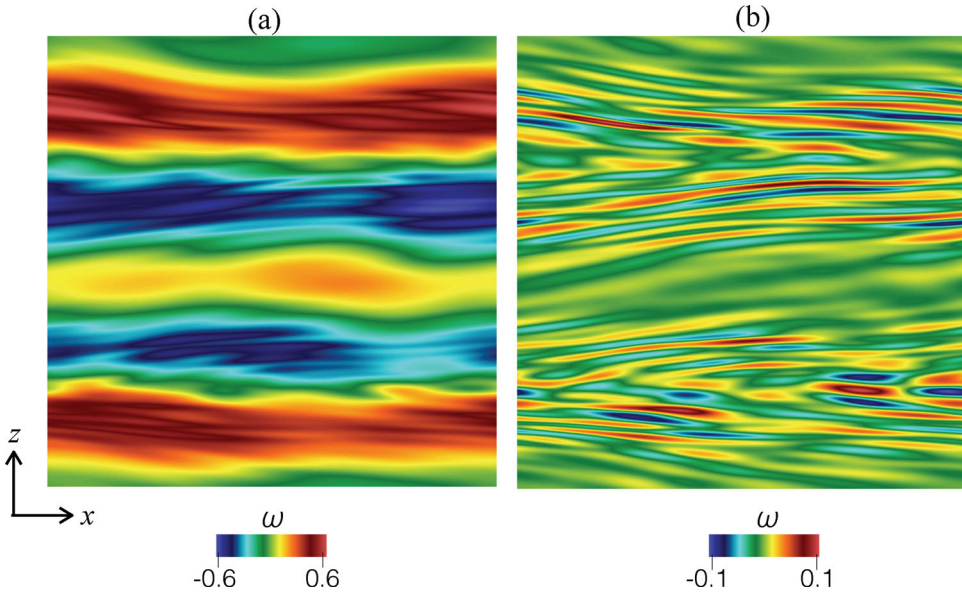


Figure 6. For $Fr = 0.16$, (a) density plot of the magnitude of vorticity field ω ; (b) The density plot of the vorticity field ω ; for this we truncate the modes in the wavenumber band $0 \leq k \leq 10$.

$E_{K_h}(k) > E_{K_v}(k)$. Further, $E_{K_h}(k) \sim k^{-3}$ and $E_{K_v}(k) \sim k^{-5}$. Indeed, the different spectral exponents of horizontal and vertical KE spectra show that the flow is anisotropic at all length scales.

So, for strong stratification, the picture that emerges is of large-scale internal gravity waves, physically manifested as a VSHF, that coexist with small-scale turbulence which is characterised by an approximate k^{-3} scaling for both the KE and PE. Moreover, the KE flux is close to zero while the PE flux is positive and closely follows a k^{-2} power-law. Thus, the total energy of the system is systematically transferred to small scales. Note that stably stratified turbulence in a channel also shows the coexistence of active turbulence and internal gravity waves [56]. The energetic dominance of the VSHF suggests strong anisotropy in the system and this is confirmed by the different scaling exponents of the horizontal and vertical KE spectra. To visualise the coexistence of the large-scale internal gravity waves and small-scale turbulence we plot the vorticity field in Figure 6(a), and the small-scale vorticity

field after removing the large-scale wavenumbers from the band $0 \leq k \leq 10$ in Figure 6(b). Clearly, we observe large-scale internal gravity waves or VSHF riding on a sea of small-scale turbulence.

4.2. Moderate stratification

Among our simulations, the density stratification is moderate for $Fr = 0.37$ and 0.45 (see Figure 2). In this subsection we will focus on $Fr = 0.37$ which is obtained for $Ra = 10^{10}$ and an energy supply rate of $\varepsilon = 0.01$. For this case, $Re = 3.7 \times 10^4$. As shown in Figure 2, the flow pattern for the above set of parameters differs significantly from that corresponding to strong stratification. In fact, there is no evidence of a VSHF in Figure 2 for $Fr = 0.37$.

With regard to turbulence phenomenology, Bolgiano [30] and Obukhov [31] (denoted by BO) were among the first to consider stably stratified flows in 3D. According to this phenomenology, for large scales, i.e. $k < k_B$,

$$E_K(k) = c_1 \left(\frac{g}{\rho_0} \right)^{4/5} \varepsilon_p^{2/5} k^{-11/5}, \quad (42)$$

$$E_P(k) = c_2 \left(\frac{g}{\rho_0} \right)^{-2/5} \varepsilon_p^{4/5} k^{-7/5}, \quad (43)$$

$$\Pi_K(k) = c_3 \left(\frac{g}{\rho_0} \right)^{6/5} \varepsilon_p^{3/5} k^{-4/5}, \quad (44)$$

$$\Pi_P(k) = \varepsilon_p = \text{constant}, \quad (45)$$

$$k_B = c_4 \left(\frac{g}{\rho_0} \right)^{3/2} \varepsilon_K^{-5/4} \varepsilon_p^{3/4}, \quad (46)$$

where c_i 's are constants, ε_K is the KE supply rate, ε_p is the PE supply rate, and k_B is the Bolgiano wavenumber. At smaller scales ($k > k_B$), BO argued that the buoyancy effects are weak, and hence Kolmogorov's spectrum is valid in this regime, i.e.

$$E_K(k) = C_u \varepsilon_K^{2/3} k^{-5/3}, \quad (47)$$

$$E_P(k) = C_\rho \varepsilon_K^{-1/3} \varepsilon_p k^{-5/3}, \quad (48)$$

$$\Pi_K(k) = \varepsilon_K = \text{constant}, \quad (49)$$

$$\Pi_P(k) = \varepsilon_p = \text{constant}, \quad (50)$$

where C_u and C_ρ are Kolmogorov's and Batchelor's constants, respectively. Note that the Bolgiano–Obukhov [30,31] scaling is valid for nearly isotropic stably stratified turbulence. The recent developments [38,57–60] in 3D stably stratified turbulence, at moderate stratification, have confirmed the existence of BO scaling. For strongly stratified turbulence, Lindborg [34] shown that the horizontal KE and PE spectra exhibit $-5/3$ spectral exponent, while the vertical KE and PE spectra exhibit -3 spectral exponent. Later, the direct numerical simulations of Brethouwer *et al.* [35] and Bartello and Tobias [36] also confirmed the Lindborg [34] scaling laws for strongly stratified turbulence.

For 2D stably stratified turbulence, Equations (47)–(50) need to be modified for the $k > k_B$ regime since 2D hydrodynamic turbulence yields k^{-3} energy spectrum at small scales

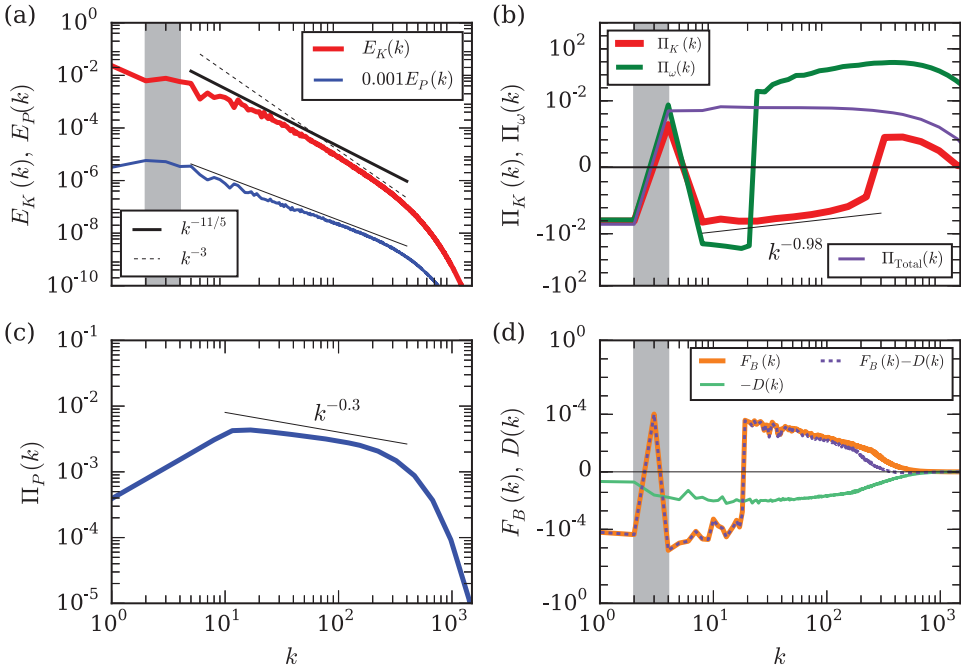


Figure 7. Moderate stratification ($Fr = 0.37$): (a) the KE and PE spectra. KE spectrum shows dual scaling with $k^{-11/5}$ and k^{-3} . The best fit for PE spectrum is $k^{-1.64}$ (thin black line); (b) KE flux $\Pi_K(k)$, enstrophy flux $\Pi_\omega(k)$, and total energy flux $\Pi_{\text{Total}}(k)$; (c) PE flux; (d) $F_B(k)$, $D(k)$, and $F_B(k) - D(k)$.

due to constant enstrophy cascade. Thus, modifications of Equations (47)–(50) take the form

$$E_K(k) = c_5 \Pi_\omega^{2/3} k^{-3}, \quad (51)$$

$$E_P(k) = c_6 k^{-1}, \quad (52)$$

$$\Pi_\omega(k) = \epsilon_\omega = \text{constant}, \quad (53)$$

$$\Pi_P(k) = \epsilon_P = \text{constant}. \quad (54)$$

Here, $\Pi_P(k) \sim k u_k \rho_k^2 = \text{const}$. As $u_k \sim k^{-1}$, this yields $\rho_k \sim \text{const}$. Hence, we argue that $E_P(k) \sim \rho_k^2 / k \sim k^{-1}$. At these smaller scales, it is important to note that the degree of non-linearity is expected to be higher for moderate stratification, which leads to $E_P(k) \sim k^{-1}$ and $\Pi_P(k) \sim \text{const}$, in contrast to $E_P(k) \sim k^{-3}$ and $\Pi_P(k) \sim k^{-2}$ for strongly stratified flows.

The KE and PE spectra as well as their fluxes are shown in Figure 7. The KE spectrum $E_K(k)$ exhibits BO scaling, in particular, $E_K(k) \sim k^{-11/5}$ for $5 \leq k \leq 90$, and $E_K(k) \sim k^{-3}$ for $90 \leq k \leq 400$. The KE flux, seen in Figure 7(b), also varies with scale; at large scales we see an inverse transfer (that scales approximately as $k^{-0.98}$) for $8 \leq k \leq 200$, while at small scales we obtain a forward transfer of KE for $200 \leq k \leq 1000$. The enstrophy flux is positive except for a narrow band near $k \approx 10$. Note that the PE spectrum (Figure 7(a)) does not show dual scaling and scales approximately as $k^{-1.64}$; its flux is also not a constant but follows $\Pi_P(k) \sim k^{-0.3}$. We note that the behaviour of KE flux does not change at the

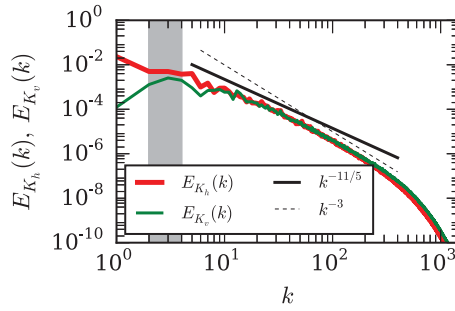


Figure 8. Plots for horizontal and vertical kinetic energy spectra for moderate stratification ($Fr = 0.37$). Both the spectra show dual scaling similar to $E_K(k)$.

same wavenumber as that of KE spectrum. At present, we believe that a higher resolution simulation is required to resolve the dual scaling issues.

At large scales, these scaling laws can be explained by replacing ϵ_P of Equations (42)–(44) with $\Pi_P(k) \sim k^{-0.3}$. This is similar to the variable flux arguments presented by Verma [46] and Verma and Reddy [61]. Specifically,

$$E_K(k) \sim k^{-0.3 \times 2/5} k^{-11/5} \sim k^{-2.32}, \quad (55)$$

$$E_P(k) \sim k^{-0.3 \times 4/5} k^{-7/5} \sim k^{-1.64}, \quad (56)$$

$$\Pi_K(k) \sim k^{-0.3 \times 3/5} k^{-4/5} \sim k^{-0.98}. \quad (57)$$

Indeed, the spectral indices obtained above match those in Figure 7 very closely.

At small scales, the KE spectrum $E_K(k) \approx 2.0 \Pi_\omega^{2/3} k^{-3}$ is associated with weaker buoyancy and constant enstrophy flux (see Figure 7(a,b)), and it is in accordance with Equation (51). Note that the spectra of the horizontal and vertical components of the flow also show dual scaling (see Figure 8), thus suggesting the presence of an approximately isotropic flow at moderate stratification. As mentioned, the PE spectrum does not exhibit dual scaling, and we do not see the k^{-1} scaling expected from Equation (52) at small scales. Though it should be noted that the PE flux is not constant but scales approximately as $k^{-0.3}$, and this implies a slightly steeper ($k^{-4/3}$) small scale PE spectrum. Indeed, a small change in scaling of this kind, i.e. -1.64 and -1.33 at large and small scales, respectively, may only be observable at a higher resolution.

The KE flux in the present 2D setting exhibits an inverse cascade, in contrast to the forward cascade in 3D [34]. Still the $k^{-11/5}$ spectrum of BO scaling is valid in 2D stably stratified turbulence due to the following reason. The energy supply due to buoyancy $F_B(k)$ and the dissipation rate $D(k)$, shown in Figure 7(d), exhibits $F_B(k) > 0$ for $k > 20$, in contrast to 3D stably stratified flows for which $F_B(k) < 0$ [38]. From Equation (31) we deduce that $|\Pi_K(k + \Delta k)| < |\Pi_K(k)|$ when $\Pi_K(k) < 0$ and $F_B(k) > 0$. Thus $|\Pi_K(k)|$ decreases with k and this yields Bolgiano scaling for the 2D moderately stratified flows. Physically, in Figure 9 we observe ascending lighter fluid for which u_z and ρ are positively correlated. This is in contrast to 3D stably stratified flows for which $F_B(k) < 0$ due to a conversion of KE to PE [38]; i.e. there u_z and ρ are anti-correlated. Finally, it should be noted that even though KE flows upscale in this 2D setting, the total energy is transferred from large to small scales as seen by the total energy flux $\Pi_{\text{Total}}(k)$ in Figure 7(b).

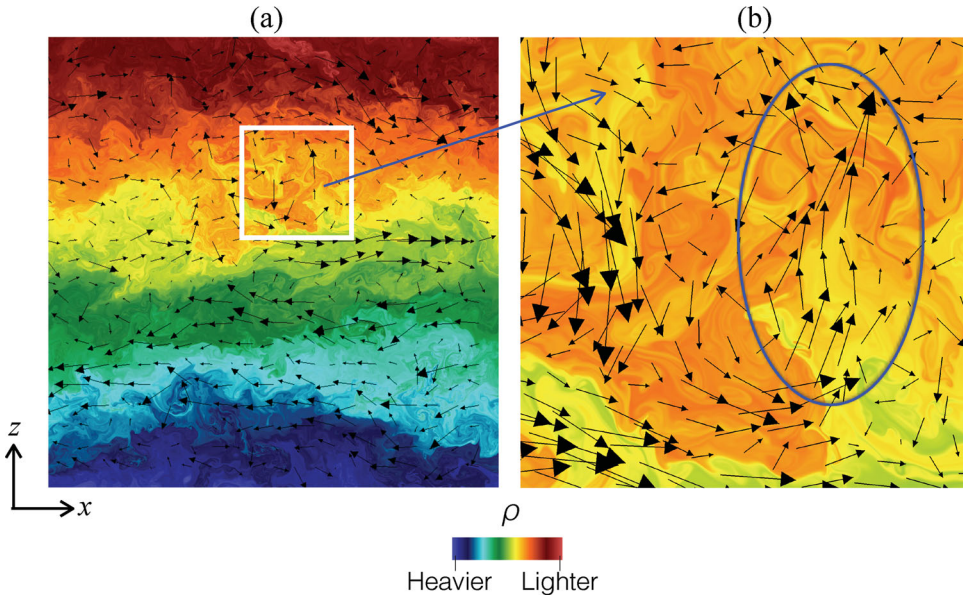


Figure 9. For $Fr = 0.37$ (a) the density plot of the density field ρ with the velocity field superimposed on it. In the boxed zone, lighter (higher) fluid ascends thus $F_b(k) \propto u_z \rho > 0$; (b) a zoomed view of the boxed zone.

4.3. Weak stratification

Finally, we discuss the flow behaviour for weak stratification. In our simulations this is achieved for $Ra = 10^8$, $\varepsilon = 0.3$ that yields $Fr = 1.1$ and $Re = 1.1 \times 10^4$. The flow pattern in [Figure 2](#) for $Fr = 1.1$ shows a complete lack of a VSHF, instead, there is a tendency to form isotropic coherent structures similar to 2D hydrodynamic turbulence [50].

The energy spectra and fluxes for this case are shown in [Figure 10](#). Qualitatively similar to the moderate stratification case, we observe a negative KE flux at large scales. The enstrophy flux is strong and always positive, in fact it increases with wavenumber and scales approximately as $k^{3/4}$ up to the dissipation scale. This feature of the enstrophy flux alters the energy spectrum as follows:

$$E_K(k) \approx \Pi_\omega^{2/3} k^3 \sim k^{3/4 \times 2/3 - 3} \sim k^{-2.5}, \tag{58}$$

which is in good agreement with our numerical finding, as shown in [Figure 10\(a\)](#). [Figure 11](#) presents the spectra of the horizontal and vertical components of the flow, both are almost identical and scale as $E_{K_h}(k)$, $E_{K_v}(k) \sim k^{-2.5}$, thus confirming isotropy at all scales for weak stratification.

The PE spectrum $E_P(k) \sim k^{-1.6}$ and its flux Π_P are approximately constant with $\Pi_P(k) \sim k^{-0.13}$. Using $E_K(k) \sim k^{-2.5}$ and $\Pi_P(k) \approx ku_k \rho_k^2 \sim k^{-0.13}$, we obtain $E_P(k) \approx \rho_k^2/k \sim k^{-1.38}$, which is a little shallower than the $k^{-1.6}$ spectrum obtained in our numerical simulation. Once again, the total energy in the system flows from large to small scales (see [Figure 10\(b\)](#)). Taken together, the behaviour of KE and PE suggests that BO scaling may still be applicable for $Fr = 1.1$, though with a very restricted shallow $(-11/5)$ large-scale KE spectrum. Indeed, it would require much higher resolution to probe this issue. Finally, we remark that for

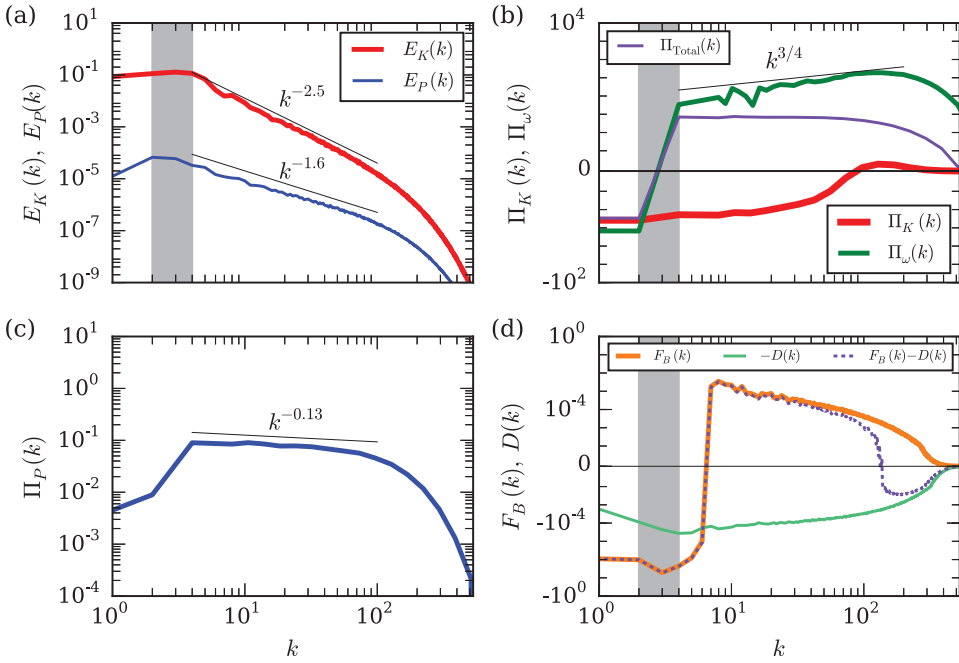


Figure 10. Weak stratification ($Fr = 1.1$); (a) plots of KE and PE spectra. KE spectrum $E_K(k)$ shows $k^{-2.5}$ scaling, while PE spectrum $E_P(k)$ shows $k^{-1.6}$ scaling; (b) plots of KE flux $\Pi_K(k)$, enstrophy flux $\Pi_\omega(k)$, and total energy flux $\Pi_{\text{Total}}(k)$; (c) PE flux $\Pi_P(k)$; (d) $F_B(k)$, $D(k)$, and $F_B(k) - D(k)$.

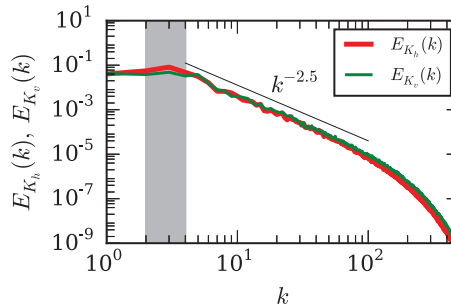


Figure 11. Plots for horizontal and vertical kinetic energy spectra for weak stratification ($Fr = 1.1$). Both the spectra, $E_{K_h}(k)$ and $E_{K_v}(k)$, overlap on each other similar to that of moderate stratification.

weakly stratified flows, the forward (inverse) transfer of PE (KE) is reminiscent of the flux loop scenario proposed by Boffetta *et al.* [27].

5. Summary and conclusions

We performed direct numerical simulations of 2D stably stratified flows under large-scale random forcing and studied the spectra and fluxes of KE, enstrophy, and PE. This is possibly the simplest non-trivial setting to explore the effects of stratification on fluid turbulence,

Table 3. Scaling of KE spectrum $E_K(k)$, PE spectrum $E_P(k)$, KE flux $\Pi_K(k)$, PE flux $\Pi_P(k)$, and enstrophy flux $\Pi_\omega(k)$ for different strength of stratification.

Strength of stratification	Spectrum	Flux
Strong	Large scale VSHF	
	Small scale turbulence: $E_K(k) \sim k^{-3}$ $E_P(k) \sim k^{-3}$	$\Pi_K(k) \sim 0$ $\Pi_\omega(k) \sim \text{const.}$ $\Pi_P(k) \sim k^{-2}$
Moderate	For $5 \leq k \leq 90$: $E_K(k) \sim k^{-2.2}$ $E_P(k) \sim k^{-1.64}$	$\Pi_K(k) \sim k^{-0.98}$ (negative) $\Pi_\omega(k) \sim \text{const.}$ $\Pi_P(k) \sim k^{-0.3}$
	For $90 \leq k \leq 400$: $E_K(k) \sim k^{-3}$ $E_P(k) \sim k^{-1.64}$	$\Pi_K(k)$: weak (positive) $\Pi_\omega(k) \sim \text{const.}$ $\Pi_P(k) \sim k^{-0.3}$
Weak	$E_K(k) \sim k^{-2.5}$ $E_P(k) \sim k^{-1.6}$	$\Pi_K(k) \sim \text{const.}$ (negative) $\Pi_\omega(k) \sim k^{3/4}$ $\Pi_P(k) \sim k^{-0.13}$

much like surface turbulence in 3D flows which allow for an examination of compressibility on energy fluxes and spectra [62]. We find that the flows exhibit remarkably different behaviour as the strength of stratification is varied, and this is summarised in Table 3.

For strong stratification, as with numerous previous studies, we observe the emergence of a large-scale VSHF. This VSHF is explicitly identified as being composed of internal gravity waves, and further is seen to coexist with smaller scale turbulence. The turbulent portion of the flow follows some aspects of the traditional enstrophy cascading regime of pure 2D turbulence. In particular, we find a strong, nearly constant, positive enstrophy flux, zero KE flux and KE spectrum that scales approximately as k^{-3} . But the PE does not act as a passive scalar. Indeed, it exhibits an approximate k^{-3} spectrum and a scale-dependent k^{-2} forward flux. In addition, the flow in the strongly stratified regime is highly anisotropic and the horizontal and vertical flow spectra follow $E_{K_h}(k) \sim k^{-3}$ and $E_{K_v}(k) \sim k^{-5}$ scaling, respectively.

Moderate stratification proves to be very interesting, specifically, there is no VSHF and we observe a modified BO scaling for the KE — $E_K(k) \sim k^{-11/5}$ at large scales and an approximate k^{-3} power-law at small scales. Further, the nature of the KE flux also changes, with the upscale or inverse transfer at large scales and a weak forward transfer at smaller scales. The PE, on the other hand, always flows downscale and its flux is weakly scale-dependent (approximately $k^{-0.3}$). The PE spectrum scales as $k^{-1.64}$, with no signs of a dual scaling like the KE. But, as the expected change in scaling of the PE spectrum is small, it is possible that higher resolution simulations may prove to be useful in this regard.

Weak stratification also differs significantly from pure 2D turbulence. In particular, we actually see a positive scale-dependent enstrophy flux ($\sim k^{3/4}$) up to the dissipation scale. In agreement with this form of the enstrophy flux, the KE spectrum scales approximately as $k^{-2.5}$. The KE flux is robustly negative, and the inverse transfer begins at a comparatively smaller scale than with moderate stratification. The PE flux, once again, is positive and almost scale-independent, and the PE spectrum follows an approximate $k^{-1.6}$ scaling law.

Thus, the nature of 2D stably stratified turbulence under large-scale random forcing is dependent on the strength of the ambient stratification. Despite this diversity, we do observe some universal features. Specifically, the total and PE always flow downscale, which is in agreement with 3D stratified turbulence. The KE almost never shows a forward transfer (apart from the weak downscale transfer at small scales in moderate stratification). In addition, the zero flux of KE and its upscale transfer at large scale for strong stratification differs from the nonzero flux for moderate and weak stratification. Finally, apart from the PE spectrum for weak stratification (and its small-scale behaviour for moderate stratification), the scaling exponents observed very closely match dimensional expectations when we take into account the scale-dependent form of the corresponding flux.

Acknowledgments

We thank Anirban Guha for useful discussions. Our numerical simulations were performed on *Chaos* clusters of IIT Kanpur and 'Shaheen IP' at KAUST supercomputing laboratory, Saudi Arabia. This work was supported by a research grant (Grant No. SERB/F/3279) from Science and Engineering Research Board, India, computational project k1052 from KAUST, and the grant PLANEX/PHY/2015239 from Indian Space Research Organisation (ISRO), India. Jai Sukhatme would also like to acknowledge support from the IISc ISRO Space Technology Cell project ISTC0352 and the Ministry of Earth Sciences Monsoon Mission grant IITM/MAS/DSG/0001.


Disclosure statement

No potential conflict of interest was reported by the authors.

Funding

Science and Engineering Research Board, India [grant number SERB/F/3279]; Computational project from King Abdullah University of Science and Technology [project number k1052]; Indian Space Research Organisation (ISRO), India [grant number PLANEX/PHY/2015239]; IISc ISRO Space Technology Cell [project number ISTC0352]; Ministry of Earth Sciences Monsoon Mission [grant number IITM/MAS/DSG/0001].

ORCID

Abhishek Kumar  <http://orcid.org/0000-0002-6026-5727>

References

- [1] Vallis GK. Atmospheric and oceanic fluid dynamics. Cambridge (UK): Cambridge University Press; 2006.
- [2] Riley J, LeLong M. Fluid motions in the presence of strong stable stratification. *Ann Rev Fluid Mech.* 2000;32:613–657.
- [3] Lilly D. Stratified turbulence and the mesoscale variability of the atmosphere. *J Atmos Sci.* 1983;40:749–761.
- [4] Hopfinger EJ. Turbulence in stratified fluids: a review. *J Geophys Res.* 1987;92:5287–5303.
- [5] Leith C. Normal mode initialization and quasigeostrophic theory. *J Atmos Sci.* 1980;37:958–968.
- [6] Embid P, Majda A. Low Froude number limiting dynamics for stably stratified flow with small or finite Rossby numbers. *Geophys Astrophys Fluid Dyn.* 1998;87:1–50.

- [7] LeLong M, Riley J. Internal wave-vortical mode interactions in strongly stratified flows. *J Fluid Mech.* **1991**;232:1–19.
- [8] Laval JP, McWilliams J, Dubrulle B. Forced stratified turbulence: successive transitions with Reynolds number. *Phys Rev E.* **2003**;68:036308.
- [9] Waite ML, Bartello P. Stratified turbulence dominated by vortical motion. *J Fluid Mech.* **2004**;517:281.
- [10] Waite ML, Bartello P. Stratified turbulence generated by internal gravity waves. *J Fluid Mech.* **2006**;546:313.
- [11] Lindborg E, Brethouwer G. Stratified turbulence forced in rotational and divergent modes. *J Fluid Mech.* **2007**;586:83–108.
- [12] Bartello P. Geostrophic adjustment and inverse cascades in rotating stratified turbulence. *J Atmos Sci.* **1995**;52:4410–4428.
- [13] Smith L, Waleffe F. Generation of slow large scales in forced rotating stratified turbulence. *J Fluid Mech.* **2002**;451:145–168.
- [14] Kitamura Y, Matsuda Y. The k_h^{-3} and $k_h^{-5/3}$ energy spectra in stratified turbulence. *Geophys Res Lett.* **2006**;33:L05809.
- [15] Sukhatme J, Smith L. Vortical and wave modes in 3D rotating stratified flows: random large-scale forcing. *Geophys Astrophys Fluid Dyn.* **2008**;102:437–455.
- [16] Vallgren A, Deusebio E, Lindborg E. Possible explanation of the atmospheric kinetic and potential energy spectra. *Phys Rev Lett.* **2011**;107:268501.
- [17] Marino R, Rosenberg D, Herbert C, et al. Interplay of waves and eddies in rotating stratified turbulence and the link with kinetic-potential energy partition. *EPL* **2015**;112:49001.
- [18] Carnevale G, Frederiksen J. A statistical dynamical theory of strongly nonlinear internal gravity waves. *Geophys Astrophys Fluid Dyn.* **1983**;23:175–207.
- [19] Frederiksen J, Bell R. Statistical dynamics of internal gravity waves - turbulence. *Geophys Astrophys Fluid Dyn.* **1983**;26:257–301.
- [20] Lvov Y, Yokoyama N. Nonlinear wave-wave interactions in stratified flows: direct numerical simulations. *Physica D.* **2009**;238:803–815.
- [21] Rempel M, Sukhatme J, Smith LM. Nonlinear gravity-wave interactions in stratified turbulence. *Theor Comput Fluid Dyn.* **2014**;28:131–145.
- [22] Benielli D, Sommeria J. Excitation of internal waves and stratified turbulence by parametric instability. *Dyn Atmos Oceans.* **1996**;23:335–343.
- [23] Bouruet-Aubertot P, Sommeria J, Staquet C. Breaking of standing internal gravity waves through two-dimensional instabilities. *J Fluid Mech.* **1995**;285:265–301.
- [24] Bouruet-Aubertot P, Sommeria J, Staquet C. Stratified turbulence produced by internal wave breaking: two-dimensional numerical experiments. *Dyn Atmos Oceans.* **1996**;23:357–369.
- [25] Sukhatme J, Smith LM. Self-similarity in decaying two-dimensional stably stratified adjustment. *Phys Fluids.* **2007**;19:036603.
- [26] Smith LM. Numerical study of two-dimensional stratified turbulence. *Contemp Math.* **2001**;283:91.
- [27] Boffetta G, de Lillo F, Mazzino A, et al. A flux loop mechanism in two-dimensional stratified turbulence. *EPL* **2011**;95:34001.
- [28] Sukhatme J, Majda AJ, Smith LM. Two-dimensional moist stratified turbulence and the emergence of vertically sheared horizontal flows. *Phys Fluids.* **2012**;24:036602–16.
- [29] Zhang J, Wu XL, Xia KQ. Density fluctuations in strongly stratified two-dimensional turbulence. *Phys Rev Lett.* **2005**;94:174503.
- [30] Bolgiano R. Turbulent spectra in a stably stratified atmosphere. *J Geophys Res.* **1959**;64:2226.
- [31] Obukhov AN. Effect of Archimedean forces on the structure of the temperature field in a turbulent flows. *Dokl Akad Nauk SSSR.* **1959**;125:1246.
- [32] Batchelor GK. Small scale variation of convected quantities like temperature in a turbulent fluid. *J Fluid Mech.* **1959**;5:113.
- [33] Seychelles F, Amarouchene Y, Bessafi M, et al. Thermal convection and emergence of isolated vortices in soap bubbles. *Phys. Rev. Lett.* **2008**;100:144501–144504.
- [34] Lindborg E. The energy cascade in a strongly stratified fluid. *J. Fluid Mech.* **2006**;550:207.

- [35] Brethouwer G, Billant P, Lindborg E, et al. Scaling analysis and simulation of strongly stratified turbulent flows. *J. Fluid Mech.* **2007**;585:343.
- [36] Bartello P, Tobias SM. Sensitivity of stratified turbulence to the buoyancy Reynolds number. *J. Fluid Mech.* **2013**;725:1–22.
- [37] Verma MK, Chatterjee AG, Reddy KS, et al. Benchmarking and scaling studies of a pseudospectral code Tarang for turbulence simulations. *Pramana.* **2013**;81:617–629.
- [38] Kumar A, Chatterjee AG, Verma MK. Energy spectrum of buoyancy-driven turbulence. *Phys Rev E.* **2014**;90:023016.
- [39] Sutherland B. *Internal gravity waves.* Cambridge (UK): Cambridge University Press; **2010**.
- [40] Lindborg E, Brethouwer G. Vertical dispersion by stratified turbulence. *J Fluid Mech.* **2008**;614:303–314.
- [41] Kraichnan R. Inertial ranges in two-dimensional turbulence. *Phys Fluids.* **1967**;10:1417.
- [42] Maltrud ME, Vallis GK. Energy spectra and coherent structures in forced two-dimensional and beta-plane turbulence. *J Fluid Mech.* **1991**;228:321.
- [43] Smith L, Yakhot V. Bose condensation and small-scale structure generation in a random force driven 2D turbulence. *Phys Rev Lett.* **1993**;71:352–355.
- [44] Borue V. Spectral exponents of enstrophy cascade in stationary two-dimensional homogeneous turbulence. *Phys Rev Lett.* **1993**;71:3967–3970.
- [45] Lindborg E, Alvelius K. The kinetic energy spectrum of the two-dimensional enstrophy turbulence cascade. *Phys Fluids.* **2000**;12:945–4.
- [46] Verma MK. Variable enstrophy flux and energy spectrum in two-dimensional turbulence with Ekman friction. *EPL* **2012**;98:14003.
- [47] Lesieur M. *Turbulence in fluids - stochastic and numerical modelling.* Dordrecht: Kluwer Academic Publishers; **2008**.
- [48] Dar G, Verma M, Eswaran V. Energy transfer in two-dimensional magnetohydrodynamic turbulence: formalism and numerical results. *Physica D.* **2001**;157:207–225.
- [49] Verma MK. Statistical theory of magnetohydrodynamic turbulence: recent results. *Phys Rep.* **2004**;401:229–380.
- [50] McWilliams J. The emergence of isolated coherent vortices in turbulent flow. *J Fluid Mech.* **1984**;146:21–43.
- [51] Billant P, Chomaz JM. Self-similarity of strongly stratified inviscid flows. *Phys Fluids.* **2001**;13:1645.
- [52] Boffetta G. Energy and enstrophy fluxes in the double cascade of two-dimensional turbulence. *J Fluid Mech.* **2007**;589:8.
- [53] Boffetta G, Musacchio S. Evidence for the double cascade scenario in two-dimensional turbulence. *Phys Rev E.* **2010**;82:016307.
- [54] Boffetta G, Ecke RE. Two-dimensional turbulence. *Annu Rev Fluid Mech.* **2012**;44:427–451.
- [55] Jullien MC, Castiglione P, Tabeling P. Experimental observation of Batchelor dispersion of passive tracers. *Phys Rev Lett.* **2000**;85:3636–3639.
- [56] Zonta F, Onorato M, Soldati A. Turbulence and internal waves in stably-stratified channel flow with temperature-dependent fluid properties. *J Fluid Mech.* **2012**;697:175–203.
- [57] Kumar A, Verma MK. Shell model for buoyancy-driven turbulence. *Phys Rev E.* **2015**;91:043014.
- [58] Verma MK, Kumar A, Chatterjee AG. Energy spectrum and flux of buoyancy-driven turbulence. *Phys Focus, AAPPs Bull.* **2015**; 25.
- [59] Bhattacharjee JK. Kolmogorov argument for the scaling of the energy spectrum in a stratified fluid. *Phys Lett A.* **2015**;379:696–699.
- [60] Rosenberg D, Pouquet A, Marino R, et al. Evidence for Bolgiano-Obukhov scaling in rotating stratified turbulence using high-resolution direct numerical simulations. *Phys Fluids.* **2015**;27:055105–25.
- [61] Verma MK, Reddy KS. Modeling quasi-static magnetohydrodynamic turbulence with variable energy flux. *Phys Fluids.* **2015**;27:025114.
- [62] Lovecchio S, Zonta F, Soldati A. Upscale energy transfer and flow topology in free-surface turbulence. *Phys Rev E.* **2015**;91:033010.